ISSN 0020-1685, Inorganic Materials, 2021, Vol. 57, No. 10, pp. 1005–1014. © Pleiades Publishing, Ltd., 2021.
Russian Text © The Author(s), 2021, published in Neorganicheskie Materialy, 2021, Vol. 57, No. 10, pp. 1063–1072.

# Synthesis and Thermal Oxidation Stability of Nanocrystalline Niobium Diboride

**S. E. Kravchenko[a], D. Yu. Kovalev[b], A. A. Vinokurov[a], N. N. Dremova[a], A. V. Ivanov[a], and S. P. Shilkin[a, *]**

[a] *Institute of Problems of Chemical Physics, Russian Academy of Sciences, Chernogolovka, Moscow oblast, 142432 Russia*

[b] *Merzhanov Institute of Structural Macrokinetics and Materials Science, Russian Academy of Sciences, Chernogolovka, Moscow oblast, 142432 Russia*

**e-mail: ssp@icp.ac.ru*

Received April 16, 2021; revised May 28, 2021; accepted June 3, 2021

**Abstract**—A method has been developed for the synthesis of nanocrystalline $NbB_2$ powder with an average particle size of 65 nm. The material has been prepared by reacting Nb and amorphous B powders (1 : 2 ratio) in $Na_2B_4O_7$, KCl, and KBr ionic melts after pretreatment with hydrogen and activation in a high-energy planetary mill for 40 min. The synthesis process was run for 32 h at 800°C in argon at a pressure of 4 MPa. The results demonstrate that, independent of the composition and nature of the melt, the process yields $NbB_2$ nanoparticles with hexagonal symmetry (sp. gr. *P*6/*mmm*) and unit-cell parameters $a = 0.3100–0.3108$ nm and $c = 0.3278–0.3298$ nm. The products of the oxidation of the $NbB_2$ nanoparticles with atmospheric oxygen during heating to 1000°C and isothermal oxidation at 400, 450, 500, 550, and 600°C have been characterized by thermal analysis, X-ray diffraction, scanning electron microscopy, energy dispersive X-ray microanalysis, X-ray photoelectron spectroscopy, and IR frustrated total internal reflection spectroscopy. The rate constants for the oxidation of $NbB_2$ nanoparticles at these temperatures have been determined to be 0.0013, 0.045, 0.47, 2.61, and 8.83 $h^{-1}$, respectively. The oxidation onset temperature has been determined to be 310°C. The effective activation energy evaluated for the oxidation of $NbB_2$ nanoparticles from the temperature dependence of rate constants is $220 \pm 8$ kJ/mol.

**Keywords:** niobium diboride, nanoparticle, high-energy mechanical treatment, ionic melt, autoclave reactor, oxidation

**DOI:** 10.1134/S002016852110006X

## INTRODUCTION

Niobium diboride, $NbB_2$, has a high melting point, good thermodynamic stability, and high hardness, strength, wear resistance, thermal and electrical conductivity, chemical inertness, and corrosion resistance, which allows it to find application in various industry sectors [1–4]. Interest in Group IV–VI metal borides has increased markedly owing to the advent of related nanocrystalline materials, whose physicochemical and mechanical properties differ significantly from those of their microcrystalline analogs [5].

Group V metal nanoparticles are typically synthesized by techniques proposed for the preparation of Group IV transition metal diborides: high-temperature solid-state elemental synthesis, borothermic reduction of various metal oxides and salts, carbothermic reduction of metal and boron oxides, magnesium reduction of metal and boron oxides, mechanochemical synthesis, chemical vapor deposition (CVD), thermolysis of appropriate metal borohydrides or their derivative complexes, and reactions of transition metal chlorides with alkali metal borohydrides without separation of transition metal borohydride derivatives at elevated temperatures and pressures [6–18].

High-temperature solid-state reaction between niobium and amorphous boron powders allows $NbB_2$ to be prepared at a high rate [6]. However, Matsudaira et al. [6] did not present any data on the purity or particle size of the synthesized niobium diboride. As shown by Peshev et al. [7] and Jha et al. [8], reaction of niobium oxides with boron at elevated temperatures in an inert atmosphere yields $NbB_2$ nanoparticles. In particular, at 1300°C in an argon atmosphere $NbO_2$ reacts with boron to form agglomerated $NbB_2$ nanorods 40 nm in diameter and 800 nm in length. Ultrafine (~50 nm) niobium diboride particles can be prepared by carbothermic reduction of niobium oxides with carbon at 1650°C [9]. Gai et al. [10] obtained $NbB_2$ nanorods 50–60 nm in diameter and up to 600 nm in length by reacting $NbCl_5$ with $NaBH_4$

in an argon atmosphere in an autoclave at temperatures in the range 550–650°C according to the scheme

$$2NbCl_5 + 4NaBH_4 \rightarrow 2NbB_2 + 6HCl + 4NaCl + 5H_2. \quad (1)$$

Ma et al. [11] obtained nanocrystalline niobium diboride with a particle size of ~30 nm by reacting Mg, $Nb_2O_5$, and $H_3BO_3$ in a mixture of molten anhydrous NaCl and $MgCl_2$ salts at a temperature of 650°C [11]. Nanocrystalline niobium diboride can be prepared by reacting $NbCl_5$ with boron and tin powders at a temperature of 700°C in a nitrogen atmosphere [12]. $NbB_2$ nanoparticles can be synthesized in the temperature range 500–900°C by reacting $NbCl_5$ with an excess of $NaBH_4$ under an argon atmosphere in a eutectic LiCl + KCl mixture [13]. Jafari et al. [14] prepared $NbB_2$ powder with a particle size of ~100 nm at 800°C by the reaction

$$3Mg + B_2O_3 + Nb \rightarrow 3MgO + NbB_2. \quad (2)$$

A mixture of magnesium, niobium, and boron oxide powders was preactivated mechanochemically. To isolate the pure $NbB_2$ obtained in reaction (2), the synthesis product containing magnesium oxide and niobium diboride was sequentially treated with hydrochloric acid, water, and ethanol [14]. Rather coarse $NbB_2$ powder, with a particle size of ~200 nm, can be prepared by magnesiothermic reduction of a mixture of niobium and boron oxides [15].

In addition, niobium diboride was prepared by chemical vapor deposition from a $NbCl_5$-, $BCl_3$-, and $H_2$-containing gas phase on a quartz substrate in the form of a homogeneous film at temperatures from 960 to 1050°C and in the form of crystals in the range 1050–1200°C [16]. According to transmission electron microscopy data, nanocrystalline $NbB_2$ with an average particle size of ~37.8 nm was obtained by reacting $Nb_2O_5$ with Mg powder and $Na_2B_4O_7 \cdot 10H_2O$ in an autoclave at 800°C [17].

Each of the above techniques has its own advantages and drawbacks. Some of them ensure a high reaction rate, whereas others make it possible to prepare niobium diboride nanoparticles of stoichiometric composition, high purity, or tailored size at relatively low temperatures, but require complex apparatus.

As an alternative approach to the preparation of $NbB_2$ nanoparticles, we propose a so-called "currentless" process [19]. Basic to this approach is "currentless" boron transport to a metal in ionic melts with various chemical compositions and structures, for example, in molten anhydrous sodium tetraborate, potassium chloride, or potassium bromide. The effect was successfully used previously in developing techniques for the synthesis of $VB_2$ and $TiB_2$ nanoparticles [20, 21]. Besides, owing to specific features of their structure and properties, the use of ionic melts as reaction media in the synthesis of Group IV–VI metal borides makes it possible to obtain metal borides in the form of nanopowders. This paper presents a direct continuation of our previous work [22].

## EXPERIMENTAL

**Starting materials.** Niobium powder 10 to 15 μm in particle size was prepared as follows: off-the-shelf niobium powder with a particle size of ~45 μm was heated at 900°C in a vacuum of 0.13 Pa and then subjected to five hydrogenation–dehydrogenation cycles as described elsewhere [23]. The residual hydrogen content of the powder was within $1.0 \times 10^{-3}$ wt % and the residual oxygen content did not exceed $3.0 \times 10^{-3}$ wt %. As a source of 99.999+%-pure hydrogen, we used a self-contained laboratory-scale hydrogen generator [23, 24] containing hydrided TiFe and $LaNi_5$ intermetallic phases as working materials. In our preparations, we also used reagent-grade potassium chloride and potassium bromide and high-purity (99.998%) argon (Russian Federation Purity Standard TU 2114-005-0024760-99). Immediately before synthesis, commercially available amorphous boron (B 99A, Russian Federation Purity Standard TU 1-92-154-90) 10 to 20 μm in particle size, potassium chloride, and potassium bromide were evacuated to a residual pressure of 0.13 Pa at a temperature of 300°C. Anhydrous sodium tetraborate was obtained by holding commercially available reagent-grade $Na_2B_4O_7 \cdot 5H_2O$ in a vacuum of 0.13 Pa at a temperature of 350°C.

**Characterization techniques.** The phase composition of the synthesized powder was determined by X-ray diffraction on a PANalytical AERIS diffractometer and a DRON-3 diffractometer with a diffracted beam monochromator. X-ray diffraction patterns were collected in step scan mode with Cu$K_\alpha$ radiation in the angular range $2\theta = 20°–110°$, with a scan step of 0.02° and a counting time per data point of 4 s. In X-ray diffraction data processing by the profile analysis method, we used Burevestnik software. Unit-cell and fine-structure parameters were evaluated using 12 reflections. Instrumental broadening was assessed from the linewidth of a $LaB_6$ reference standard (SRM 660b). The average crystallite (coherent scattering domain) size was evaluated using the method of second moments. Thermodynamic calculations of the state of the Nb–B–O system were performed with the ASTRA 4 program [25, 26].

The thermal properties of the powder were studied by simultaneous thermal analysis in combination with mass-spectrometric analysis of decomposition products, using a Netzsch STA 409 PC Luxx thermoanalytical system and a QVS 403 C Aeolos mass spectrometer, at a constant heating rate of 10°C/min under

flowing high-purity argon or air in the temperature range from 20 to 1000°C. The composition of the air was determined using an MI-1201V mass-spectrometer.

The samples were also examined by electron microscopy and energy dispersive X-ray (EDX) analysis using a combination of instruments comprising a Zeiss Supra 25 field emission scanning electron microscope and an INCA X-sight X-ray spectrometer system. Electron-microscopic images were obtained at low electron beam accelerating voltages (~4 kV). At such accelerating voltages, the contribution of the substrate to the measured signal was negligible, if any. EDX analysis data were collected at an accelerating voltage of ~8 kV.

IR frustrated total internal reflection (FTIR) spectra were measured in the range from 500 to 4000 $cm^{-1}$ using a PerkinElmer Spectrum 100 Fourier transform spectrometer and a Vertex 70V spectrometer, both equipped with accessories for taking reflection spectra.

X-ray photoelectron spectra were measured on a Specs spectrometer with an analyzer. The spectra were excited using a Mg$K_\alpha$ X-ray source ($h\nu$ = 1253.6 eV). The residual pressure in the vacuum chamber of the spectrometer during the measurements was $4 \times 10^{-7}$ Pa. The power of the source was 225 W.

The specific surface area ($S$) of the samples was determined at liquid nitrogen temperature using a Quadrasorb SI analyzer. From the $S$ measurement results, we evaluated the average diameter of the $NbB_2$ particles under the assumption that the particles were spherical in shape, using the well-known formula $d_x = 6/(\gamma S)$, where $d_x$ is the particle size and $\gamma$ is the X-ray density of $NbB_2$ (6.93 g/$cm^3$).

Hydrogen and oxygen were determined using a CHNS/O Vario Micro cube element analyzer. Chloride and bromide ions, boron, and niobium were determined by standard analytical techniques and EDX analysis.

**Experimental procedure.** The Nb powder and amorphous B in the molar ratio 1 : 2 were mixed in a Pulverisette 6 planetary mill (10-mm-diameter $ZrO_2$ balls, ball-to-powder weight ratio of 1 : 10, vial rotation rate of 400 rpm, milling time of 40 min) under an argon atmosphere at room temperature.

The resultant mixture of the Nb (9.21 g) and B (2.16 g) powders was loaded into a silica ampule together with 14.0 g of $Na_2B_4O_7$, KCl, or KBr. The ampule was then placed in a stainless steel autoclave reactor. The reactor was pumped down to a residual pressure of 0.13 Pa and filled with argon to a pressure of 4 MPa. Isothermal annealing was performed at a temperature of 800°C for 32 h. The synthesis temperature was chosen proceeding from the melting points of KCl (776°C), KBr (734°C), and $Na_2B_4O_7$ (742°C). After cooling, the sinter cake was comminuted, and the resultant powder was sequentially treated with distilled water, ethanol, and acetone. Next, the ampule was pumped down to a residual pressure of 0.13 Pa at a temperature of 50°C. After that, the synthesized powder was placed in the reactor, evacuated, and exposed to flowing hydrogen under a pressure of 5 MPa at a temperature of 100°C for 4 h. After cooling, the powder was withdrawn from the reactor in an argon atmosphere.

**Table 1.** Composition and unit-cell parameters of $NbB_2$ prepared in $Na_2B_4O_7$, KCl, and KBr ionic melts

| Ionic melt | Chemical composition of the product* | $a$, nm | $c$, nm |
|---|---|---|---|
| $Na_2B_4O_7$ | $NbB_{1.97}O_{0.02}$ | 0.3100 | 0.3278 |
| KCl | $NbB_{2.01}O_{0.01}$ | 0.3104 | 0.3295 |
| KBr | $NbB_{2.02}O_{0.03}$ | 0.3108 | 0.3298 |

* According to X-ray photoelectron spectroscopy data, oxygen was located in the surface layer of the $NbB_2$ nanoparticles in the form of niobium(V) and boron oxides [22].

The isothermal oxidation of the $NbB_2$ nanoparticles with atmospheric oxygen was carried out at temperatures of 400, 450, 500, 550, 600, and 700°C in an tubular quartz reactor 20 mm in diameter and 300 mm in length (150-mm-long heating zone), heated by a standard demountable laboratory-scale electric furnace. The samples were placed in a platinum foil boat. The temperature in the reactor was maintained by a PT200 temperature controller with an accuracy of ±2°C and was measured by a Chromel–Alumel thermocouple. The maximum holding time of the samples at the above temperatures was 6 h. The air flow rate in the reactor was 30 mL/min. The degree of conversion, $\alpha$, was evaluated as the ratio of the observed increase in the weight of the $NbB_2$ sample over a given period of time to the maximum possible one, calculated for the $NbB_2$ oxidation reaction

$$2NbB_2 + 5.5O_2 \rightarrow Nb_2O_5 + 2B_2O_3. \quad (3)$$

## RESULTS AND DISCUSSION

Table 1 summarizes our results on the chemical and phase compositions of the material obtained in $Na_2B_4O_7$, KCl, and KBr ionic melts. According to the chemical and EDX analysis data, the composition of the synthesized material was $NbB_{1.97-2.02}O_{0.01-0.03}$, independent of the ionic melt used. A typical X-ray diffraction pattern of the powder (Fig. 1) indicates that the synthesis product is single-phase and consists of crystalline $NbB_2$ (hexagonal symmetry, sp. gr.

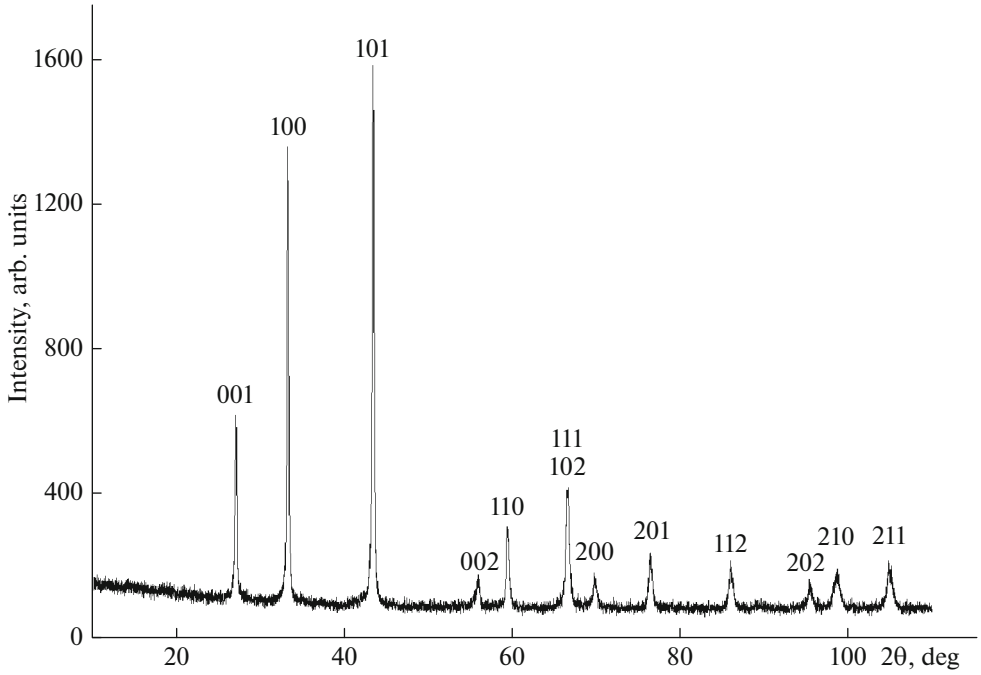


**Fig. 1.** X-ray diffraction pattern of the $NbB_2$ nanoparticles prepared in a KBr ionic melt.

*P*6/*mmm*). No considerable amounts of impurity phases were detected. The unit-cell parameters of $NbB_2$ (Table 1) agree with those reported previously [27], including those indicated in the ICDD diffraction database (PDF-2, card no. 000-35-0742).

According to scanning electron microscopy (SEM) data, the $NbB_2$ nanoparticles prepared in ionic melts differed in shape, but most of them were spherical. The average particle size was determined to be 64–67 nm (Fig. 2, Table 2), and the particles were agglomerated.

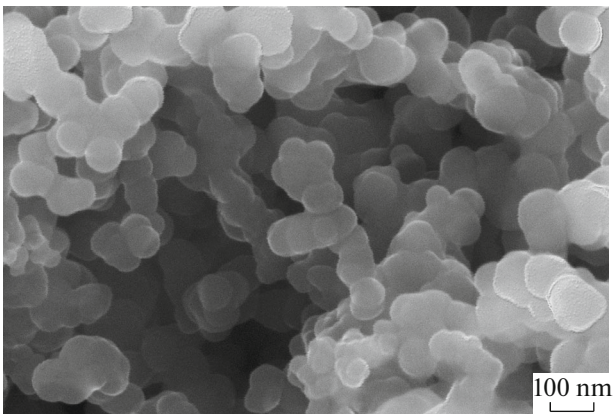


**Fig. 2.** Electron micrograph of the $NbB_2$ nanoparticles prepared in a KBr ionic melt.

Table 2 compares the average $NbB_2$ particle sizes evaluated from SEM data, X-ray diffraction profile analysis, and specific surface area measurements. The results obtained by the different methods demonstrate that the average $NbB_2$ particle size is 65 nm, independent of the nature of the ionic melt (Table 2). In the temperature range 20–1000°C under an argon atmosphere, $NbB_2$ undergoes no transformations involving heat release or absorption or weight changes.

According to previous work [19–21], the observed B transport to Nb in $Na_2B_4O_7$, KCl, and KBr melts can be accounted for by the formation of $B^{2+}$, lower valence ions, by the reaction

$$B + 2B^{3+}_{melt} \rightarrow 3B^{2+}_{melt} \quad (4)$$

which then react with niobium to form $NbB_2$ by the reaction

$$3B^{2+}_{melt} + Nb \rightarrow B^{3+}_{melt} + NbB_2. \quad (5)$$

**Oxidation of $NbB_2$ nanoparticles.** To study the oxidation of $NbB_2$ nanoparticles, we performed thermodynamic calculations of the state of the system with an initial Nb : B : O molar ratio of 1 : 2 : 5.5 (reaction (3)) in the temperature range 300–1000°C at atmospheric pressure. In the calculations, we used thermodynamic data for $NbB_2$ from Bolgar et al. [28]. According to the calculation results, essentially the only equilibrium products in the condensed phase are $B_2O_3$ and $Nb_2O_5$.

**Table 2.** Average size of the $NbB_2$ nanoparticles prepared in $Na_2B_4O_7$, KCl, and KBr ionic melts

| Ionic melt | Average particle size, nm (SEM data) | Crystallite size, nm | Average particle size from *S* data, nm |
|---|---|---|---|
| $Na_2B_4O_7$ | 65 | 60 | 67 ($S = 13.0$ m$^2$/g) |
| KCl | 64 | 59 | 67 ($S = 13.0$ m$^2$/g) |
| KBr | 67 | 57 | 62 ($S = 14.0$ m$^2$/g) |

The equilibrium concentrations of the lower boron and niobium oxides are negligible.

Figure 3 presents thermal analysis results for the oxidation of the $NbB_2$ nanoparticles during heating in the range 20–1000°C. The oxidation onset temperature of the $NbB_2$ nanoparticles was 310°C. For the oxidation onset temperature of $NbB_2$ we took the temperature at which the sample weight increased by 0.1 wt %. The differential thermal analysis (DTA) curve of the sample contains an exothermic peak at 574°C, due to the formation of $Nb_2O_5$ and $B_2O_3$ by reaction (3). According to X-ray diffraction data, the $NbB_2$ oxidation products consisted of only the niobium oxide $Nb_2O_5$ (Fig. 4g).

Figures 4a–4g show X-ray diffraction patterns of the products of isothermal oxidation at temperatures of 400, 450, 500, 550, 600, and 700°C and oxidation during heating to 1000°C for the $NbB_2$ nanoparticles prepared in a KBr ionic melt. In the temperature range studied, the X-ray diffraction patterns show only reflections from $Nb_2O_5$ and $NbB_2$. The $B_2O_3$ phase forming by reaction (3) is probably amorphous. At 400°C, the phase composition of the powder remains unchanged, even though there is a slight weight gain (Fig. 4a). Reflections from the $Nb_2O_5$ phase emerge in the X-ray diffraction patterns at 450°C (Fig. 4b). At temperatures above 550°C (Figs. 4d–4g), the powder contains only the oxide phase, and there are no reflections from $NbB_2$.

Figure 5 shows the B 1*s* X-ray photoelectron spectrum of the oxidation products of the $NbB_2$ nanoparticles after isothermal annealing at 700°C. The B 1*s* peak position (194.0 eV) indicates the presence of boric anhydride or boric acid in the oxidation products [29, 30]. The IR FTIR spectroscopy results in Fig. 6 lend support to the former assumption. The IR spectrum of the oxidation products of the $NbB_2$ nanoparticles is essentially identical to the spectrum of boric anhydride [31] and has no lines characteristic of $H_3BO_3$ (at 3200, 1450, or 1196 cm$^{-1}$) [32].

Figure 7 illustrates the morphology of the oxidation products of the $NbB_2$ nanoparticles obtained at

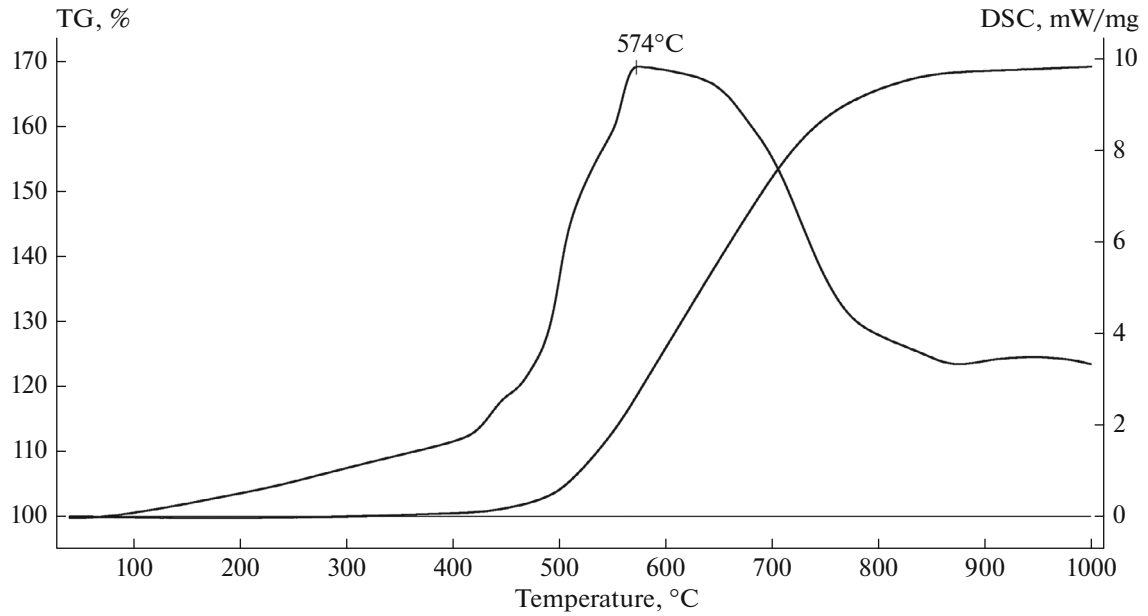


**Fig. 3.** Thermal analysis results for the oxidation of the $NbB_2$ nanoparticles prepared in a KBr ionic melt.

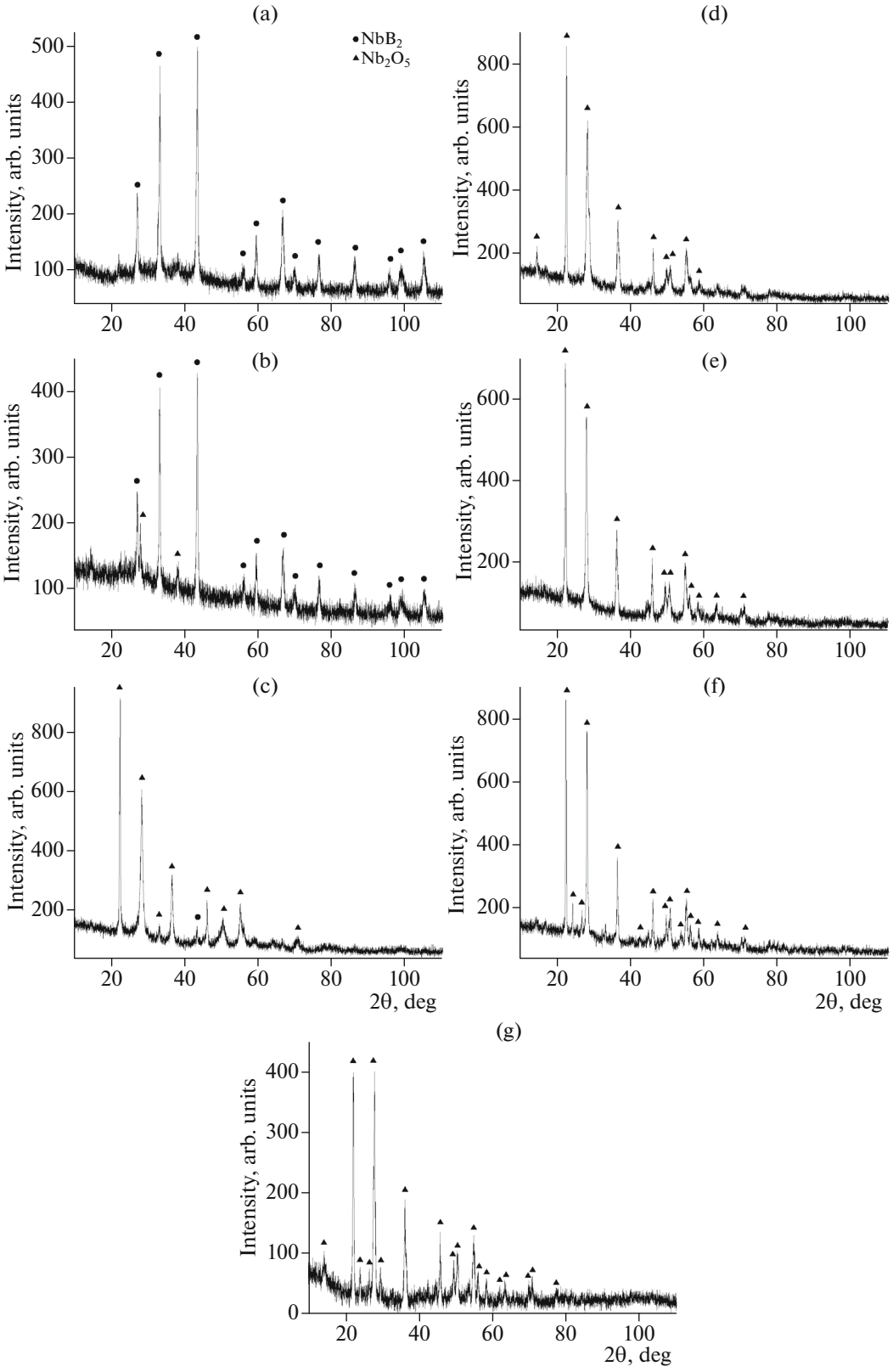


**Fig. 4.** X-ray diffraction patterns of the oxidation products of the $NbB_2$ nanoparticles prepared in a KBr ionic melt: isothermal oxidation in flowing air at temperatures of 400 (a), 450 (b), 500 (c), 550 (d), 600 (e), and 700°C (f) and oxidation during heating to 1000°C (g).

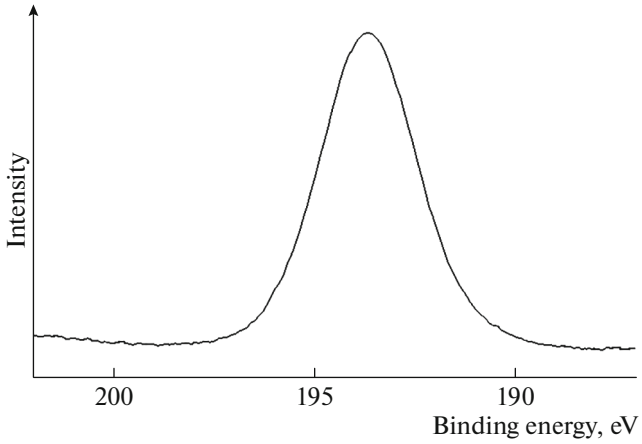


**Fig. 5.** B 1*s* X-ray photoelectron spectrum of the oxidation products of the $NbB_2$ nanoparticles after isothermal annealing at 700°C.

various oxidation temperatures. Comparison with the starting powder (Fig. 2) demonstrates that the morphology of the nanoparticles depends on the heating temperature in flowing air. According to the X-ray diffraction, EDX analysis, and chemical analysis data, the oxidation products were free from nitrogen-containing niobium and boron derivatives.

The weight gain calculated for the complete oxidation of $NbB_2$ according to scheme (3) is 76.86%. The weight gain of our samples during heating was considerably smaller (Fig. 3). This may be due to both diffusion hindrance to the oxidation by reaction products or the volatility of boron oxide, which has melting and boiling points of ~450 and ~2250°C, respectively. According to mass spectrometry data, the released gas phase contains a considerable amount of $B_2O_3$ at temperatures above 700°C.

Figure 8 shows kinetic curves for the oxidation of $NbB_2$ nanoparticles at various temperatures. The kinetic curve can be described by the Avrami–Erofeev equation

$$[-\ln(1-\alpha)]^{1/n} = k\tau,$$

where $\alpha$ is the degree of conversion, $k$ is the rate constant, and $\tau$ is time. The value of $n$ was found to be 1/2, characteristic of gas–solid heterogeneous processes. The kinetic curves have well-defined nonlinearity: after a sharp weight change during an initial period of time, the oxidation of the $NbB_2$ nanoparticles is then "hindered."

The calculated degree of conversion at temperatures above 600°C is markedly influenced by the vaporization of the $B_2O_3$ formed. After holding for 1–2 h, the sample weight is determined by the formation of oxidation reaction products (weight gain) and concurrent $B_2O_3$ vaporization (weight loss). With increasing reaction temperature and time, the latter process begins to prevail, leading to an apparent decrease in the calculated degree of conversion. Because of this, the rate constant for the oxidation of the $NbB_2$ nanoparticles were evaluated from the slope of the initial portion of the kinetic curves. The reaction rate

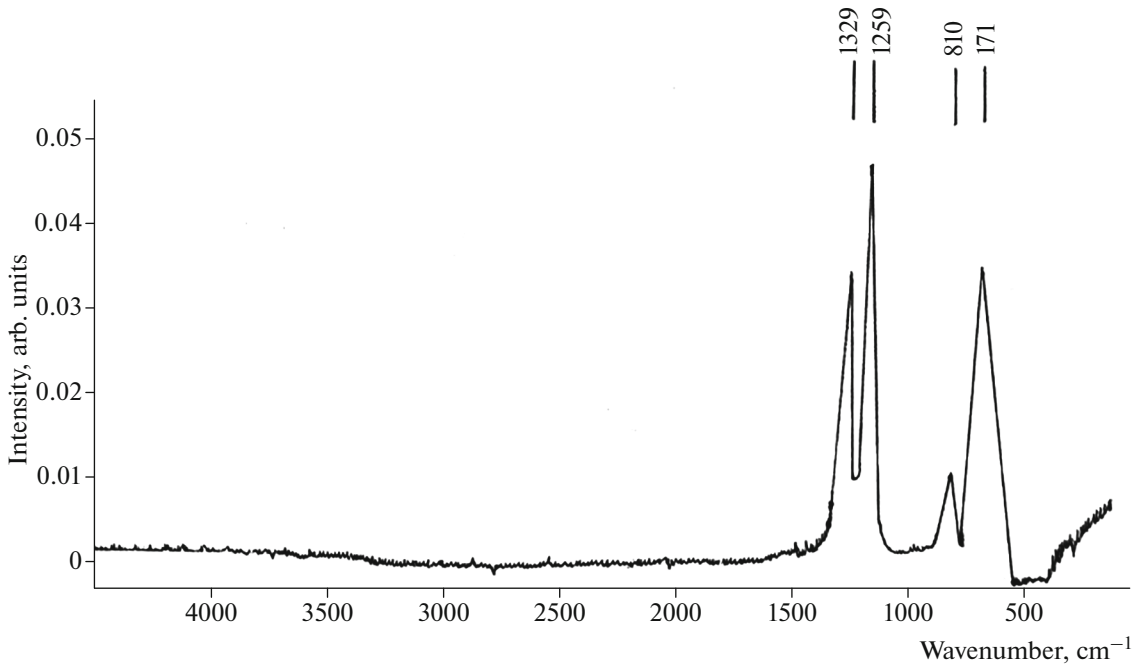


**Fig. 6.** IR FTIR spectrum of the oxidation products of the $NbB_2$ nanoparticles after isothermal annealing at 700°C.

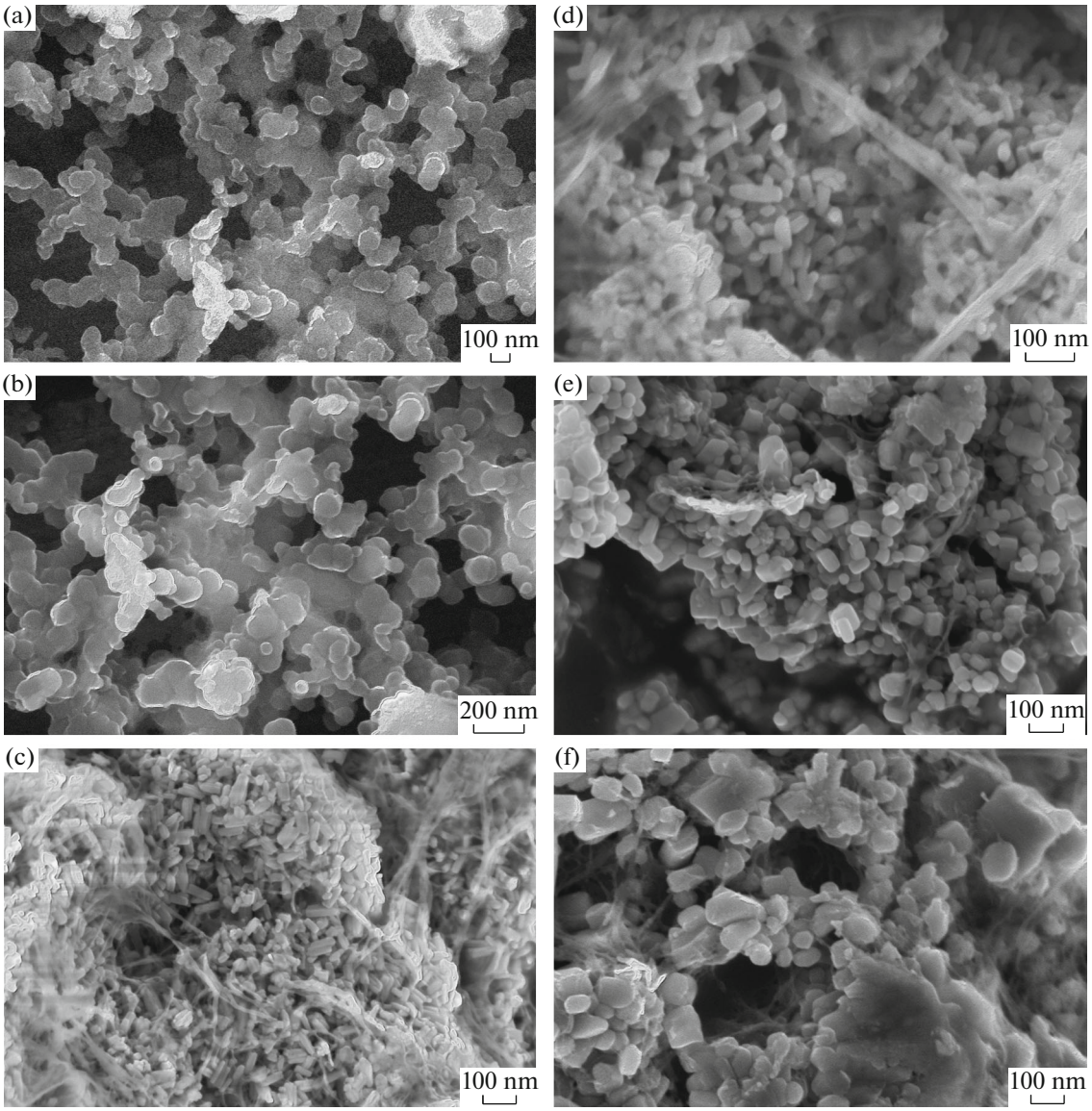


**Fig. 7.** Morphology of the nanoparticles prepared in a KBr ionic melt an then oxidized at temperatures of (a) 400, (b) 450, (c) 500, (d) 550, (e) 600, and (f) 700°C.

constants for $NbB_2$ oxidation at temperatures of 400, 450, 500, 550, and 600°C were determined to be 0.0013, 0.045, 0.47, 2.61, and 8.83 $h^{-1}$, respectively. The effective activation energy evaluated for $NbB_2$ oxidation reaction from the temperature dependence of rate constants in the temperature range 400–600°C was 220 ± 8 kJ/mol.

## CONCLUSIONS

We have studied interaction between Nb and B powders (1 : 2) at a temperature of 800°C, argon pressure of 4 MPa, and reaction time of 32 h in $Na_2B_4O_7$, KCl, and KBr ionic melts after pretreatment with hydrogen and activation in a high-energy planetary mill for 40 min. The results demonstrate that, independent of the composition and nature of the melt, the process yields single-phase nanocrystalline $NbB_2$ with an average particle size of ~65 nm. The synthesized $NbB_2$ has hexagonal symmetry, space group *P*6/*mmm*, with unit-cell parameters $a = 0.3100–0.3108$ nm and $c = 0.3278–0.3298$ nm.

The products of oxidation of $NbB_2$ nanoparticles with atmospheric oxygen during heating to 1000°C and isothermal oxidation at 400, 450, 500, 550, and 600°C have been characterized by physicochemical analysis techniques. The rate constants for the oxidation of $NbB_2$ nanoparticles at these temperatures have been determined to be 0.0013, 0.045, 0.47, 2.61, and

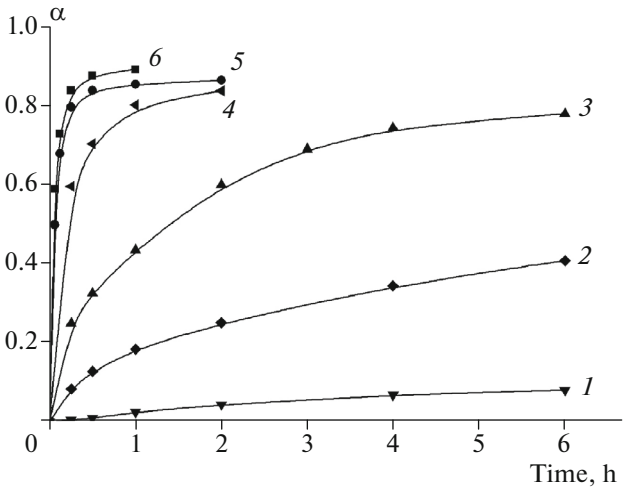


**Fig. 8.** Degree of conversion α as a function of oxidation time for the $NbB_2$ nanoparticles at oxidation temperatures of (*1*) 400, (*2*) 450, (*3*) 500, (*4*) 550, (*5*) 600, and (*6*) 700°C.

8.83 $h^{-1}$, respectively. The oxidation onset temperature has been determined to be 310°C. The effective activation energy evaluated for the oxidation of $NbB_2$ nanoparticles in the temperature range 400–600°C from the temperature dependence of oxidation rate constants is 220 ± 8 kJ/mol.

## ACKNOWLEDGMENTS

In this study, we used equipment at the Shared Analytical Facilities Center, Institute of Problems of Chemical Physics, Russian Academy of Sciences, and at the Shared Research Facilities Center, Merzhanov Institute of Structural Macrokinetics and Materials Science, Russian Academy of Sciences.

## FUNDING

This work was supported by the Russian Federation Ministry of Science and Higher Education, state research targets for the Institute of Problems of Chemical Physics, Russian Academy of Sciences (theme state registration no. AAAA-A19-119061890019-5) and the Merzhanov Institute of Structural Macrokinetics and Materials Science, Russian Academy of Sciences (theme no. 44.1).

## REFERENCES

1. Serebryakova, T.I., Neronov, V.A., and Peshev, P.D., *Vysokotemperaturnye boridy* (High-Temperature Borides), Chelyabinsk: Metallurgiya, 1991.
2. Carenco, S., Portehault, D., Boissiere, C., Mezailles, N., and Sanchez, C., Nanoscaled metal borides and phosphides: recent developments and perspectives, *Chem. Rev.,* 2013, vol. 113, no. 10, pp. 7981–8065. https://doi.org/10.1021/cr400020d
3. Andrievskii, R.A. and Spivak, I.I., *Prochnost' tugoplavkikh soedinenii i materialov na ikh osnove. Spravochnik* (Strength of Refractory Compounds and Related Materials: A Handbook), Chelyabinsk: Metallurgiya, 1989.
4. Prokhorov, A.M., Lyakishev, N.P., Burkhanov, G.S., and Dement'ev, V.A., High-purity transition-metal borides: promising materials for present-day technology, *Inorg. Mater.,* 1996, vol. 32, no. 11, pp. 1195–1201.
5. Andrievski, R.A. and Khatchoyan, A.V., *Nanomaterials in Extreme Environments, Fundamentals and Applications,* Berlin: Springer, 2016. https://doi.org/10.1007/978-3-319-2533-2
6. Matsudaira, T., Itoh, H., and Naka, S., Synthesis of niobium boride powder by solid-state reaction between niobium and amorphous boron, *J. Less-Common Met.,* 1989, vol. 155, no. 2, pp. 207–214. https://doi.org/10.1016/0022-5088(89)90229-4
7. Peshev, P., Leyarovska, L., and Bliznakov, G., On the borothermic preparation of some vanadium, niobium and tantalum borides, *J. Less-Common Met.,* 1968, vol. 15, pp. 259–267. https://doi.org/10.1016/0022-5088(68)90184-7
8. Jha, M., Ramanujachary, K.V., Lofland, S.E., Gupta, G., and Ganguli, A.K., Novel borothermal process for the synthesis of nanocrystalline oxides and borides of niobium, *J. Dalton Trans.,* 2011, vol. 40, pp. 7879–7888. https://doi.org/10.1039/c1dt10468c
9. Maeda, H., Yoshikawa, T., Kusakabe, K., and Morooka, S., Synthesis of ultrafine $NbB_2$ powder by rapid carbothermal reduction in a vertical tubular reactor, *J. Alloys Compd.,* 1994, vol. 215, pp. 127–334. https://doi.org/10.1016/0925-8388(94)90829-X
10. Gai, P., Yang, Z., Shi, L., Chen, L., Zhao, A., Gu, Y., and Qian, Y., Low temperature synthesis of $NbB_2$ nanorods by a solid-state reaction route, *Mater. Lett.,* 2005, vol. 59, pp. 3550–3552. https://doi.org/10.1016/j.matlet.2005.07.051
11. Ma, J., Du, Y., Wu, M., Li, G., Feng, Z., Guo, M., Sun, Y., Song, W., Lin, M., and Guo, X., A simple inorganic-solvent route to nanocrystalline niobium diboride, *J. Alloys Compd.,* 2009, vol. 468, pp. 473–476. https://doi.org/10.1016/j.jallcom.2008.01.021
12. Jothi, P.R., Yubuta, K., and Fokwa, B.P.T., A simple, general synthetic route toward nanoscale transition metal borides, *Adv. Mater.,* 2018, vol. 30, no. 14, paper 1704181. https://doi.org/10.1002/adma.201704181
13. Portehaut, D., Devis, S., Beaunier, P., Gervais, C., Giordano, C., Sanchez, C., and Antonietti, M., A general solution route toward metal boride nanocrystals, *Angew. Chem.,* 2011, vol. 50, pp. 3262–3265. https://doi.org/10.1002/ange.201006810
14. Jafari, M., Tajizadegan, H., Golabgir, M.H., Chami, A., and Torabio, O., Investigation on mechanochemical behavior of Al/Mg–$B_2O_3$–Nb system reactive mixtures to synthesize niobium diboride, *J. Refract. Met. Hard Mater.,* 2015, vol. 50, pp. 86–92. https://doi.org/10.1016/j.ijrmhm.2014.10.017
15. Balci, Ö., Ağaoğullari, D., Övecoğlu, M.L., and Duman, I., Synthesis of niobium borides by powder metallurgy methods using $Nb_2O_5$, $B_2O_3$ and Mg blends,

*Trans. Nonferrous Met. Soc. China,* 2016, vol. 26, pp. 747–758.
https://doi.org/10.1016/S1003-6326(16)64165-1

16. Motojima, S., Sugiyama, K., and Takahashi, Y., Chemical vapor deposition of niobium diboride ($NbB_2$), *J. Cryst. Growth,* 1975, vol. 30, pp. 233–239.
https://doi.org/10.1016/0022-0248(75)90094-9
17. Kravchenko, S.E., Torbov, V.I., and Shilkin, S.P., Nanosized zirconium diboride: synthesis and properties, *Russ. J. Inorg. Chem.,* 2011, vol. 56, no. 4, pp. 506–509.
https://doi.org/10.1134/S0036023611040164
18. Gupta, A., Singhal, V., and Pandey, O.P., Facile in-situ synthesis of $NbB_2$ nanoparticles at low temperature, *J. Alloys Compd.,* 2018, vol. 736, pp. 306–313.
https://doi.org/10.1016/j.jallcom.2017.10.257
19. Ilyushchenko, N.G., Anfinogenov, A.I., and Shurov, N.I., *Vzaimodeistvie metallov v ionnykh rasplavakh* (Interactions between Metals in Ionic Melts), Moscow: Nauka, 1991.
20. Kravchenko, S.E., Domashnev, I.A., Dremova, N.N., Vinokurov, A.A., and Shilkin, S.P., Synthesis of vanadium diboride nanoparticles via reaction of amorphous boron with vanadium in KCl and $Na_2B_4O_7$ ionic melts, *Inorg. Mater.,* 2019, vol. 55, no. 5, pp. 443–448.
https://doi.org/10.1134/S002016851905011X
21. Volkova, L.S., Shulga, Yu.M., and Shilkin, S.P., Synthesis of nano-sized titanium diboride in a melt of anhydrous sodium tetraborate, *Russ. J. Gen. Chem.*, 2012, vol. 82, no. 5, pp. 819–821.
https://doi.org/10.1134/S1070363212050027
22. Kravchenko, S.E., Vinokurov, A.A., Dremova, N.N., Nadkhina, S.E., and Shilkin, S.P., Synthesis of niobium diboride nanoparticles by the reaction of amorphous boron with niobium in KCl and $Na_2B_4O_7$ ionic melts, *Russ. J. Gen. Chem.*, 2021, vol. 91, no. 2, pp. 302–304.
https://doi.org/10.1134/S1070363221020195
23. Fokin, V.N., Fokina, E.E., and Shilkin, S.P., Synthesis of coarsely crystalline metal hydrides, *Russ. J. Gen. Chem.,* 1996, vol. 66, no. 8, pp. 1210–1212.
24. Fokin, V.N., Fokina, E.E., Tarasov, B.P., and Shilkin, S.P., Synthesis of the tetragonal titanium dihydride in ultradispersed state, *Int. J. Hydrogen Energy*, 1999, vol. 24, nos. 2–3, pp. 111–114.
https://doi.org/10.1016/S0360-3199(98)00070-6
25. Trusov, B.G., Thermodynamic analysis of high-temperature states and processes and its practical implementation, *Doctoral (Eng.) Dissertation,* Moscow: Moscow State Tech. Univ., 1984.
26. Sinyarev, G.B., Vasolin, N.A., Trusov, B.G., and Moiseev, G.K., *Primenenie EVM dlya termodinamicheskikh raschetov metallurgicheskikh protsessov* (Use of Computers for Thermodynamic Evaluation of Metallurgical Processes), Moscow: Nauka, 1982.
27. *Diagrammy sostoyaniya dvoinykh metallicheskikh sistem: Spravochnik (Phase Diagrams of Binary Metallic Systems: A Handbook)*, Lyakishev, N.P., Ed., Moscow: Mashinostroenie, 1996, vol. 1.
28. Bolgar, A.S., Serbova, M.I., Fesenko, V.V., Serebryakova, T.I., and Isaeva, L.P., High-temperature enthalpy and heat capacity of niobium diboride, *Teplofiz. Vys. Temp.,* 1980, vol. 18, no. 6, pp. 1180–1183.
29. Joyner, D.J. and Hercules, D.M., Chemical bonding and electronic structure of $B_2O_3$, $H_3BO_3$, and BN: ESCA, Auger, SIMS and SXS study, *J. Chem. Phys.,* 1980, vol. 72, no. 2, pp. 1095–1108.
https://doi.org/10.1063/1.439251
30. Ong, C.W., Huang, H., Zheng, B., Kwok, R.W.M., Hui, Y.Y., and Lau, W.M., X-ray photoemission spectroscopy of nonmetallic materials: electronic structures of boron and $B_xO_y$, *J. Appl. Phys.,* 2004, vol. 95, no. 7, pp. 3527–3534.
https://doi.org/10.1063/1.1651321
31. Sidorov, T.A. and Sobolev, N.N., Infrared and Raman spectra of boric anhydride: III. Interpretation of the vibrational spectrum of boric anhydride and calculation of the isotopic effect, *Opt. Spektrosk.,* 1958, vol. 4, no. 1, pp. 9–16.
32. Bethell, D.E. and Sheppard, N., The infrared spectrum and structure of boric oxide, *Trans. Faraday Soc.,* 1955, vol. 51, pp. 9–15.

*Translated by O. Tsarev*